NASA TECHNICAL NOTE

NASA TN D-6223

SUPERSONIC ASYMMETRIC FLUTTER AND DIVERGENCE OF TRUNCATED CONICAL SHELLS WITH RING-SUPPORTED EDGES

by Sidney C. Dixon and M. Latrelle Hudson

Langley Research Center
Hampton, Va. 23365

NATIONAL AERONAUTICS AND SPACE ADMINISTRATION • WASHINGTON, D. C. • MAY 1971

1. Report No.	2. Government Accession No.	3. Recipient's Catalog No.
NASA TN D-6223		

4. Title and Subtitle

SUPERSONIC ASYMMETRIC FLUTTER AND DIVERGENCE OF TRUNCATED CONICAL SHELLS WITH RING-SUPPORTED EDGES

5. Report Date: May 1971

6. Performing Organization Code:

7. Author(s): Sidney C. Dixon and M. Latrelle Hudson

8. Performing Organization Report No.: L-7527

9. Performing Organization Name and Address:

NASA Langley Research Center
Hampton, Va. 23365

10. Work Unit No.: 124-08-20-04

11. Contract or Grant No.:

12. Sponsoring Agency Name and Address:

National Aeronautics and Space Administration
Washington, D.C. 20546

13. Type of Report and Period Covered: Technical Note

14. Sponsoring Agency Code:

15. Supplementary Notes:

16. Abstract

The flutter of truncated conical shells supported at the ends by rings was studied analytically. The basic flutter characteristics were determined, and the effects of shell geometry on these characteristics were investigated. Three types of flow-induced instabilities were found: flutter in two circumferential waves, divergence in two circumferential waves, and flutter in many circumferential waves. For end rings that were not very stiff, the instabilities could occur at dynamic pressures that were orders of magnitude less than the values obtained for shells with simple or clamped edge support. For shells free of external static loading, prevention of divergence required the stiffest end rings for small cone angles and prevention of flutter in two circumferential waves required the stiffest end rings for large cone angles. Flutter in many circumferential waves was the critical mode of instability for all cone angles when the end rings were very stiff. This type of flutter occurred at dynamic pressures approaching the values required for shells with simple or clamped edge support. For shells subjected to static external-pressure loads, divergence governed design conditions for small values of cone angle, flutter for moderate values of cone angle, and buckling for large values of cone angle.

Calculations were made for two aeroshell designs which had minimum weight from a buckling point of view. The aeroelastic calculations indicated that the possibility of flutter or divergence of these aeroshells during a Mars landing was remote.

17. Key Words (Suggested by Author(s))	18. Distribution Statement
Conical-shell flutter Ring-supported shells	Unclassified – Unlimited

19. Security Classif. (of this report)	20. Security Classif. (of this page)	21. No. of Pages	22. Price*
Unclassified	Unclassified	24	$3.00

*For sale by the National Technical Information Service, Springfield, Virginia 22151

SUPERSONIC ASYMMETRIC FLUTTER AND DIVERGENCE OF TRUNCATED CONICAL SHELLS WITH RING-SUPPORTED EDGES

By Sidney C. Dixon and M. Latrelle Hudson
Langley Research Center

SUMMARY

The flutter of truncated conical shells supported at the ends by rings was studied analytically. The basic flutter characteristics were determined, and the effects of shell geometry on these characteristics were investigated. Three types of flow-induced instabilities were found: flutter in two circumferential waves, divergence in two circumferential waves, and flutter in many circumferential waves. For end rings that were not very stiff, the instabilities could occur at dynamic pressures that were orders of magnitude less than the values obtained for shells with simple or clamped edge support. For shells free of external static loading, prevention of divergence required the stiffest end rings for small cone angles and prevention of flutter in two circumferential waves required the stiffest end rings for large cone angles. Flutter in many circumferential waves was the critical mode of instability for all cone angles when the end rings were very stiff. This type of flutter occurred at dynamic pressures approaching the values required for shells with simple or clamped edge support. For shells subjected to static external-pressure loads, divergence governed design conditions for small values of cone angle, flutter for moderate values of cone angle, and buckling for large values of cone angle.

Calculations were made for two aeroshell designs which had minimum weight from a buckling point of view. The aeroelastic calculations indicated that the possibility of flutter or divergence of these aeroshells during a Mars landing was remote.

INTRODUCTION

Ring stiffeners are often used to provide end support for shells of revolution in aerospace applications, such as planetary entry vehicles. (See refs. 1 and 2.) Recently, there has been considerable research effort on the buckling of ring-supported shells (see, for example, refs. 1 and 3 to 10) and some research on the vibration characteristics of ring-supported shells (see, for example, refs. 11 and 12). However, virtually no information exists on the flutter characteristics of ring-shell configurations.

In the present investigation, the analysis of reference 8 is used to determine the flutter and divergence characteristics of ring-supported truncated conical shells. The analysis of reference 8 is based on linear Donnell-type shell theory, and the aerodynamic loading is represented by the inviscid two-dimensional quasi-steady approximation (modified piston theory). In-plane inertias and structural damping are neglected. The governing equations are solved by an assumed displacement method.

Numerical results are presented to indicate the significant trends for the flutter of isotropic ring-supported conical shells, including the effects of end-ring stiffness, shell geometry, and external-pressure loading. In addition, results for two blunt-cone aeroshells typical of planetary-entry-vehicle designs are presented.

SYMBOLS

Measurements and calculations were made in the U.S. Customary Units. They are presented herein in the International System of Units (SI) with the equivalent values given parenthetically in the U.S. Customary Units. The appendix presents factors relating these two systems of units.

A cross-sectional area of ring

$C_p = R_1^3 \frac{p}{D}$

c speed of sound in air

c_m speed of sound in cone material

D bending stiffness

d interior-ring spacing

E Young's modulus

G shear modulus

g_a aerodynamic damping coefficient, $g_a = \rho_l c_l / \gamma \omega_r$

h_c core depth of sandwich construction

h_f face-sheet thickness of sandwich construction

h_w wall thickness of shell of single-sheet construction

I_x, I_y, I_{xy} centroidal moments and product of inertia of ring cross section

J torsional stiffness of ring

L height of conical frustum

M Mach number

n number of circumferential waves

p static pressure load on shell (positive for external pressure)

q dynamic pressure of air flow

R end radius of conical frustum (see fig. 1)

r cross-sectional radius of circular end ring

t thickness of end ring

x,y Cartesian coordinates (see fig. 2)

z_c distance from neutral axis of sheet-ring combination to middle surface of conical shell

z_o eccentricity of end-ring centroidal axis measured from shell middle surface (positive for external ring)

z_s distance from neutral axis of sheet-ring combination to centroid of ring

α semivertex angle of cone

$\beta = \sqrt{M_l^2 - 1}$

γ shell mass per unit area

λ flutter parameter, $\lambda = 2q_l R_1^3/\beta D$

μ Poisson's ratio

ρ air density

ω circular frequency

$\phi = \left(q_l/\beta E\right)^{1/3}\left(R/h_w\right)$

ω_r reference frequency, $\omega_r^2 = D/\gamma R_1^4$

Subscripts:

1 small end of cone or first natural frequency

2 large end of cone or second natural frequency

3 third natural frequency

l local conditions

∞ free-stream conditions

PROBLEM, SOLUTION, AND ASSUMPTIONS

The configuration studied in this investigation consists of a truncated conical shell supported at the ends by rings. (See fig. 1.) Only thin-wall rings with circular cross sections are considered; the pertinent dimensions and stiffness properties assumed in this investigation are given in figure 2. Since the radii at the ends of a conical shell $\left(R_1 \text{ and } R_2\right)$ differ, the required stiffness properties of the two end rings can also be expected to differ. An approximate relationship between the two different end rings was established in reference 10 on the basis of minimum-weight rings sufficiently stiff to provide the equivalent of essentially clamped support for buckling of shell-ring configurations. The relationship is

$$r_1/r_2 = t_1/t_2 = R_1/R_2 \tag{1}$$

where r and t are the ring cross-section radius and thickness, respectively. The ring proportions used in the calculations of this investigation satisfy equation (1). The flutter

and divergence characteristics of the shell-ring configurations are determined for various combinations of shell geometry, ring stiffness, and external-pressure loading.

Numerical results were obtained from a computer program based on the analysis of reference 8, which uses linear Donnell-type shell theory and a membrane prestress state. The aerodynamic loading is represented by the inviscid two-dimensional quasi-steady approximation (modified piston theory). In-plane inertias and structural damping are neglected. Expressions relating the stiffness and mass characteristics of the end rings to the ring and shell material properties and geometry were obtained from equations (A5) to (A8) of reference 11. In the analysis of reference 8, coupled governing equations for the stress function and normal displacement were obtained from the principle of virtual work. The displacement was assumed, the equation for the stress function was solved exactly in terms of the coefficients of the assumed displacement, and then the equation for the displacement was solved by the generalized Galerkin method. Up to 40 terms were used in this investigation to insure convergence of results. Calculations were assumed to be converged when the results for $N + 4$ terms differed by less than 1 percent from the results for N terms.

Flutter analysis of cylindrical shells with simply supported edges (ref. 13) has revealed that if the effects of structural damping and in-plane inertias are considered the critical stability boundary is generally the flutter boundary resulting from coalescence of the first two longitudinal modes of vibration $(\omega_1 - \omega_2)$. This type of flutter, which has many circumferential waves and is relatively insensitive to the effects of structural damping and in-plane inertias, is the only type that has been observed experimentally. (See ref. 14.) If the effects of structural damping and in-plane inertia are neglected, however, higher mode flutter boundaries (usually for $n = 0$) are the critical theoretical stability boundaries; this type of flutter is very sensitive to the effects of structural damping and in-plane inertia. In view of the flutter trends for cylindrical shells and the fact that the analysis used herein neglects the effects of structural damping and in-plane inertia, numerical results are presented only for asymmetric ($n \geqq 2$) flutter resulting from coalescence of the first two longitudinal modes; usually this type of flutter was the critical flutter instability. Although the quantitative results for $n = 2$ are questionable because of the use of Donnell theory, the trends are considered to be correct since the theory yields correct trends for buckling and vibration of ring-supported shells. (See refs. 8, 10, and 12.)

RESULTS AND DISCUSSION

Aeroelastic Characteristics of Ring-Supported Shells

The flutter characteristics of a shell-ring configuration are shown in figure 3 in terms of the flutter parameter λ, where $\lambda = 2q_l R_1^3/\beta D$, and the ring-shell-radius

ratios $(r/R)_1 = (r/R)_2$ for the shell properties given in the figure. The solid curves in figure 3 are for rings of the same material mass density as the shell, and the dashed curve is for massless rings. Results for shells with clamped and simply supported edges are also shown. The curves in figure 3 indicate four distinct regions, one stable and three unstable. The unstable regions are flutter for $n = 2$, divergence for $n = 2$, and flutter for $n = 12$. The mass of the end rings had essentially no effect on divergence for $n = 2$ or on flutter for $n = 12$, but had a significant effect on flutter for $n = 2$.

Buckling results for the shell considered in figure 3 subjected to hydrostatic-pressure loading are shown in figure 4 in terms of the pressure parameter C_p where $C_p = R_1^3 \frac{p}{D}$ and the ring-shell-radius ratios. As can be seen from figures 3 and 4, there is a definite similarity in the effects of ring stiffness on the buckling and on the flutter characteristics of shell-ring configurations. When the end rings are not very stiff, the shell buckles or flutters in an $n = 2$ mode at values of C_p or λ that vary considerably with ring stiffness (size) and that can be orders of magnitude less than the values for clamped edges. When the end rings are very stiff, the shell buckles or flutters in a $n > 2$ mode at values of C_p and λ that are influenced only slightly by ring stiffness and that are bracketed by the results for simply supported and clamped ends.

Determination of the minimum ring stiffness required for suppression of the $n = 2$ mode of buckling as the critical instability of the shell-ring configuration has been used as the design criterion for end rings of proposed planetary entry vehicles. (See, for example, ref. 15.) Such a criterion results in rings that provide edge restraint between simple and clamped support and results in a minimum shell-ring configuration mass (ref. 10) on the basis of buckling. However, it has been shown both theoretically and experimentally (ref. 12) that rings sized to provide such edge restraint on the basis of buckling considerations do not provide the equivalent edge restraint on the basis of vibration considerations. This phenomenon is illustrated in figure 5, which gives the variation of the frequency ratio $(\omega_1/\omega_r)^2$ with wave number n for the shell considered in figures 3 and 4 with end rings having a ring-shell-radius ratio of 0.021. This ratio corresponds to the minimum value required to prevent the $n = 2$ mode of buckling. (See fig. 4.) The effect of ring mass on the frequency results (ω_1) is not significant, in contrast to its effect on the flutter results for $n = 2$. (See fig. 3.) As can be seen from figure 5, the values of $(\omega_1/\omega_r)^2$ for ring-supported edges are less than the values for simple and clamped edge support for $n < 4$ by over an order of magnitude. Also for $n = 2$, the shell flutters at a value of λ that is less than the value for simple or clamped edge support by more than an order of magnitude. (See fig. 3.) Thus, a ring sized to provide edge restraint between simple and clamped support on the basis of buckling does not provide the equivalent edge restraint on the basis of either vibration or flutter.

The flutter region for $n = 2$ is bounded; this rather peculiar behavior is illustrated in figure 6, where the variation of the flutter parameter λ with the frequency ratio $(\omega/\omega_r)^2$ for $(r/R)_1 = (r/R)_2 = 0.021$ and $n = 2$ is shown. As λ is increased from zero, the first two natural frequencies ω_1 and ω_2 are real and approach each other until at some critical value of λ they coalesce. For further increase in λ, the frequencies become complex and the shell flutters; the real part of the complex frequencies is the flutter frequency and is indicated by the dashed line in figure 6. This behavior is typical of plate and shell flutter instabilities based on modified piston theory aerodynamics. (See, for example, ref. 16.) However, with further increases in λ, flutter stops and the frequencies again become real and distinct; ω_1 decreases and ω_2 increases as λ increases. Finally, a value of λ is reached for which $\omega_1 = 0$ which infers loss of static stability; such a condition induced by airflow is termed divergence.

The peculiar start-stop behavior of the $n = 2$ flutter and its sensitivity to ring mass raise the question as to whether this flutter is a weak instability that might be eliminated by considering the effects of such physical realities as damping. The effects of aerodynamic damping are shown in figure 7 in terms of the flutter parameter λ and the aerodynamic damping coefficient g_a. The solid curve represents the variation with λ of the value of g_a required to suppress flutter as calculated from the flutter analysis. The dashed curve represents the variation of g_a with λ for aluminum at sea level at $M_l = 3$ and was obtained from the relation of reference 8.

$$g_a = \frac{0.662}{(1 - \mu^2)^{1/6}} \left[\frac{\rho_l}{\gamma/h_w} \frac{c_{m,l}}{c_l} \frac{M_l^2 - 1}{M_l^4} \right]^{1/3} \lambda^{2/3} \tag{2}$$

Curves for denser materials or higher altitudes would fall to the left of the dashed curve shown. Flutter occurs when the value of g_a required to suppress flutter (solid curve) exceeds the value given by equation (2) for the specified material, altitude, and Mach number (dashed curve). As can be seen, for the specified conditions damping has a slight stabilizing effect on the value of λ at flutter start (about 10 percent greater than for no damping), and has a somewhat larger affect on the value of λ at flutter stop (about 20 percent less than for no damping). However, the results clearly indicate that the instability is strong.

Effects of Shell Geometry

The results of figures 3 to 7 are for a particular shell geometry. Additional calculations thus were made to determine the influence of cone angle α and radius-thickness ratio R_1/h_w on the flutter characteristics of shell-ring configurations.

Cone angle.- Figure 8 shows the variation of λ with $(r/R)_1 = (r/R)_2$ for the same shell considered in figure 3 but with different cone angles α. The results of figure 3 are for $\alpha = 30^o$; the results of figure 8 are for $\alpha = 10^o$ (fig. 8(a)) and $\alpha = 45^o$ (fig. 8(b)). Although these results are similar to the results of figure 3, the size of the bounded $n = 2$ flutter region is seen to be related to cone angle. The results suggest this region would be nonexistent or at most very small for cylindrical shells ($\alpha = 0^o$).

The upper bound of the $n = 2$ flutter region is not shown for $\alpha = 45^o$ (fig. 8(b)) and for ring-shell-radius ratios greater than 0.035. Flutter occurred up to values of $\lambda = 10^5$ and greater values of λ were not considered. Note that when α is small ($\alpha = 10^o$), the critical instability for weak rings in general is divergence (fig. 8(a)), whereas for $\alpha = 30^o$ and 45^o the critical instability is flutter (figs. 3 and 8(b)).

The symbols and dashed curves in figure 8(a) indicate flutter boundaries for $n = 7$, $n = 8$, and $n = 9$ which for certain ranges of the ring-shell-radius ratio fall below the critical stability boundary. The characteristics of this type of flutter are indicated in figure 9, which shows the variation of the flutter parameter λ with the frequency ratio $(\omega/\omega_r)^2$ for $r/R = 0.03$ and $n = 9$. As λ is increased from zero, the first two frequencies are real and approach each other until they coalesce. For further increase in λ, the frequencies become complex and the shell flutters; the real part of the complex frequencies is the flutter frequency and is indicated by the dashed line in figure 9. With further increases in λ the mode 1-2 flutter stops and the frequencies again become real and distinct. The frequency ω_1 remains relatively insensitive to further increases in λ, whereas the frequency ω_2 increases and eventually coalesces with the frequency ω_3. Thus, whereas the $n = 2$ instabilities indicated a mode 1-2 flutter start, mode 1-2 flutter stop, and a mode 1 divergence sequence (fig. 6), the $n = 9$ instability indicates a mode 1-2 flutter start, a mode 1-2 flutter stop, and a mode 2-3 flutter start sequence.

The strength of the $n = 9$ instability is indicated in figure 10, which shows the effects of aerodynamic damping. The solid curve represents the variation of g_a with λ calculated from the flutter analysis, and the dashed lines represent the variation obtained from equation (2) for aluminum at sea level and steel at 30.5 km (100 000 feet) at $M = 3$. As can be seen, the mode 1-2 flutter for $n = 9$ is extremely sensitive to aerodynamic damping, and this type of flutter would not even occur for aluminum shells at sea level; hence, the instability was termed weak flutter (fig. 8(a)) and was not considered a significant part of the overall flutter characteristics of shell-ring configurations.

Figure 11 shows the variation with cone angle of the minimum value of ring-shell-radius ratio required to suppress the $n = 2$ mode as the governing instability for the shell properties given in the figure. As can be seen, prevention of $n = 2$ divergence requires the largest (stiffest) end rings for α up to about 30^o and prevention of $n = 2$

flutter requires the largest end rings for α greater than about 30°. Further, rings sized to prevent the $n = 2$ type of buckling are inadequate to prevent the critical flow-induced $n = 2$ instability for the entire range of α considered.

Radius-thickness ratio.- Calculations for values of R_1/h_w up to 1000 indicated that the variation of λ with ring-shell-radius ratio was similar to the variation for $R_1/h_w = 200$ shown in figure 3. Figure 12 shows the variation with radius-thickness ratio of the minimum ring-shell-radius ratio required to suppress the $n = 2$ mode as the governing instability for the shell properties given in the figure. As can be seen, prevention of the $n = 2$ flutter instability requires the largest (stiffest) end rings for the entire range of R_1/h_w considered. Note, however, that for $R_1/h_w \geqq 200$, the value of ring-shell-radius ratio only slightly exceeds the value required to prevent $n = 2$ divergence. Again, rings sized to prevent the $n = 2$ type of buckling are inadequate to prevent flow-induced $n = 2$ instabilities for the entire range of R_1/h_w considered.

Effects of External Pressure

The results presented in figures 11 and 12 indicate the end-ring sizes required to prevent the three types of instabilities, flutter, divergence, and buckling. However, in the calculations for flutter and divergence, the effects of external static loading were neglected, and in the calculations for buckling, the effects of airflow were neglected. Furthermore, these results do not reveal which type of instability would first be encountered under various flight conditions and, hence, be the governing factor in shell and end-ring design.

To gain some insight into which types of instabilities might govern design, calculations were made in which the combined effects of static and aerodynamic pressure loadings were considered. The calculations were made for conical shells subjected to supersonic airflow and a pressure drag which was assumed to be reacted by a compressive axial load acting at the large end of the shell.

Results for $\alpha = 10^{\circ}$, 30°, and 45° are shown in figure 13 in terms of λ and C_p. Following the usual design criterion for end rings (ref. 15), the calculations were made for values of the radius ratio corresponding to the value for which the buckling pressures in the $n = 2$ and $n > 2$ modes are equal. Shell and ring properties are given in the figures.

If the internal pressure of the shells is taken to be zero, the differential pressure acting on the shells is then equal to the external pressure, and λ and C_p are related by

$$\lambda = \frac{2}{\beta} \frac{q_l}{q_\infty} \frac{q_\infty}{p} C_p \tag{3}$$

If the truncated conical shell is assumed to have a pointed conical forebody, the quantities q_l/q_∞ and q_∞/p can be obtained with the aid of the conical flow charts of reference 17 for various values of α and M_∞.

The dashed lines in figure 13 indicate the variation of λ with C_p as given by equation (3) for various values of M_∞. The region bounded by these lines is the region for which the local flow over the cone is supersonic $(M_l > 1.1)$. For internal pressures greater than zero, the slopes of the dashed lines would increase because C_p would then be smaller for a given value of external pressure.

For $\alpha = 10^\circ$ (fig. 13(a)), there are two types of instability, divergence and buckling, and divergence governs design for all flow conditions shown. For $\alpha = 30^\circ$ and 45°, there are also two types of instability, buckling and flutter. For these large cone angles, flutter is the critical flow-induced instability. Flutter governs design for all flow conditions shown for $\alpha = 30^\circ$ (fig. 13(b)), whereas buckling governs the design for $\alpha = 45^\circ$ (fig. 13(c)).

The trends shown in figure 13 might change somewhat with variations in shell geometry $(L/R_1$ and $R_1/h_w)$ and type of loading. Furthermore, increases in end-ring size would have only a slight effect on the buckling results but considerable effect on the divergence and flutter results. Nevertheless, the results of figures 3, 8, and 13 suggest that for conical shells subjected to supersonic airflow divergence governs design for small values of α, flutter for moderate values of α, and buckling for large values of α. Thus, prevention of the $n = 2$ mode of buckling which was used in reference 15 as a criterion for the design of the end rings for blunt-cone planetary entry vehicles ($\alpha = 60^\circ$) appears to be appropriate.

Flutter of Typical Aeroshells

Essentially all structural studies of aeroshells for planetary entry vehicles have used end rings designed on the basis of buckling considerations. (See, for example, ref. 15.) The results of the previous section suggest that for these blunt-cone configurations such a design criterion is appropriate. However, it would be of interest to consider the flutter of typical proposed aeroshells to determine what flutter margins might exist. Two of the optimum structural designs presented in reference 15 were analyzed for flutter. The pertinent shell and ring dimensions and properties used in the calculations were obtained from Gerald A. Cohen of Philco-Ford Corporation (now at Structures Research Associates, Newport Beach, California). These dimensions and properties are given in table I for an orthotropic ring-stiffened shell and for an isotropic sandwich shell. The ring-stiffened shell had variable ring size and spacing; in this investigation an average size and spacing was assumed. The zee-section rings were assumed to have a constant developed width

(flanges and web) equal to the average developed width of the actual rings. An average spacing was assumed so that the shell had the same number of rings as the actual shell.

The flutter results are shown in the following table:

Construction	Edge support	q_l/β, kN/m^2 (psf)	
		Present investigation	Ref. 2 (ϕ=7)
Sandwich	Rings	965 (20 150)	1283 (26 800)
Ring stiffened	Free	318 (6 650)	
Ring stiffened	Rings	326 (6 800)	
Ring stiffened	Simply supported	2787 (58 200)	

Results for the isotropic sandwich shell are compared with the flutter criterion suggested in reference 2,

$$\phi = \left(q_l/\beta E\right)^{1/3}\left(R/h_w\right) \tag{4}$$

The following critical values of ϕ were defined in reference 2:

$$\left.\begin{aligned} \phi_{crit} &= 7.0 \text{ (cylinders)} \\ \phi_{crit} &= 12.7 \text{ (curved panel)} \end{aligned}\right\} \tag{5}$$

For the present study, h_w was replaced by the equivalent value for sandwich construction, ϕ_{crit} was conservatively taken equal to 7, and R was taken to be R_2.

As can be seen from the preceding table, the calculated value of q_l/β for the isotropic sandwich shell is about 75 percent of the value given by equations (4) and (5). Results for the ring-stiffened shell are presented for three types of edge restraint: free, ring supported, and simply supported. The value of q_l/β for ring-supported edges is only about 2 percent larger than the value for free edges and is nearly an order of magnitude less than the value for supported edges. However, for planetary exploration such as Mars landings, the peak free-stream dynamic pressures expected are of the order of 11.0 kN/m^2 (230 psf). (See ref. 15.) In addition, for a blunt cone supersonic flow occurs over only a small part of the shell even at an angle of attack. The results of figure 13(c) suggest that the effects of lateral-pressure loading would not have a significant, if any, degrading effect on the flutter characteristics of the shells. Although the limited experimental data on flutter of conical shells (ref. 18) indicate the theory is unconservative by over a factor of 2, the margin of safety indicated by the numerical results presented in the

table is extremely large. Hence, it must be concluded that a flutter problem for aeroshells seems remote; a similar conclusion was reached in reference 2.

CONCLUDING REMARKS

The flutter of truncated conical shells supported at the ends by rings has been studied analytically. The basic flutter characteristics were determined, and the effects of shell geometry on these characteristics were investigated. Three types of flow-induced instabilities were found: flutter in two circumferential waves, divergence in two circumferential waves, and flutter in many circumferential waves. For end rings that were not very stiff it was shown that the instabilities could occur at dynamic pressures that were orders of magnitude less than the values obtained for shells with simple and clamped edge support. For shells free of external static loading, prevention of divergence required the stiffest end rings for small cone angles and prevention of flutter in two circumferential waves required the stiffest end rings for large cone angles. Flutter in many circumferential waves was the critical mode of instability for all cone angles when the end rings were very stiff. This type of flutter occurred at dynamic pressures approaching the values required for shells with simple or clamped edge support. For shells subjected to static external-pressure loads, divergence governed design conditions for small values of cone angle, flutter for moderate values of cone angle, and buckling for large values of cone angle. Calculations were made for two structural designs obtained in another investigation for blunt-cone type aeroshell planetary entry vehicles. The designs were minimum weight from a buckling point of view. The aeroelastic calculations indicated that the possibility of flutter or divergence of aeroshells during a Mars landing is remote.

Langley Research Center,
National Aeronautics and Space Administration,
Hampton, Va., March 25, 1971.

APPENDIX A

CONVERSION OF U.S. CUSTOMARY UNITS TO SI UNITS

The International System of Units (SI) was adopted by the eleventh General Conference on Weights and Measures, Paris, October 1960 in resolution No. 12 (ref. 19). Conversion factors for the units used herein are given in the following table:

Physical quantity	U.S. Customary Unit	Conversion factor (*)	SI Unit
Area	$inch^2$ (in^2)	0.6452×10^{-3}	$meters^2$ (m^2)
Force	pounds force (lbf)	4.448	newtons (N)
Length	inches (in.)	0.0254	meters (m)
Mass	pounds mass (lbm)	0.4536	kilograms (kg)
Moment of inertia	$inch^4$ (in^4)	0.4162×10^{-6}	$meters^4$ (m^4)
Young's modulus	pounds force/$inch^2$ (lbf/in^2)	6.895×10^3	newtons/$meter^2$ (N/m^2)
Pressure	pounds force/$foot^2$ (lbf/ft^2)	47.88	newtons/$meter^2$ (N/m^2)

*Multiply value given in U.S. Customary Unit by conversion factor to obtain equivalent value in SI Unit.

Prefixes to indicate multiple of units are as follows:

Prefix	Multiple
giga (G)	10^9
kilo (k)	10^3
centi (c)	10^{-2}
milli (m)	10^{-3}

REFERENCES

1. Cohen, Gerald A.: The Effect of Edge Constraint on the Buckling of Sandwich and Ring-Stiffened 120 Degree Conical Shells Subjected to External Pressure. NASA CR-795, 1967.

2. Menkes, E. G.; and Houbolt, J. C.: Evaluation of Aerothermoelasticity Problems for Unmanned Mars-Entry Vehicles. J. Spacecraft Rockets, vol. 6, no. 2, Feb. 1969, pp. 178-184.

3. Cohen, Gerald A.: Buckling of Axially Compressed Cylindrical Shells With Ring-Stiffened Edges. AIAA J., vol. 4, no. 10, Oct. 1966, pp. 1859-1862.

4. Wang, Leon Ru-Liang: Effects of Edge Restraint on the Stability of Spherical Caps. AIAA J., vol. 4, no. 4, April 1966, pp. 718-719.

5. Almroth, B. O.; and Bushnell, D.: Computer Analysis of Various Shells of Revolution. AIAA J., vol. 6, no. 10, Oct. 1968, pp. 1848-1855.

6. Bushnell, David: Buckling of Spherical Shells Ring-Supported at the Edges. AIAA J., vol. 5, no. 11, Nov. 1967, pp. 2041-2046.

7. Bushnell, David: Inextensional Buckling of Spherical Shells With Edge Rings. AIAA J., vol. 6, no. 2, Feb. 1968, pp. 361-364.

8. Dixon, Sidney C.; and Hudson, M. Latrelle: Flutter, Vibration, and Buckling of Truncated Orthotropic Conical Shells With Generalized Elastic Edge Restraint. NASA TN D-5759, 1970.

9. Dixon, Sidney C.; Weeks, George E.; and Anderson, Melvin S.: Effects of Edge-Restraint Coupling on Buckling of Ring-Supported Cylinders. AIAA J., vol. 6, no. 8, Aug. 1968, pp. 1602-1604.

10. Dixon, Sidney C.; and Carine, John B.: Preliminary Design Procedure for End Rings of Isotropic Conical Shells Loaded by External Pressure. NASA TN D-5980, 1970.

11. Cohen, Gerald A.: Computer Analysis of Asymmetric Free Vibrations of Ring-Stiffened Orthotropic Shells of Revolution. AIAA J., vol. 3, no. 12, Dec. 1965, pp. 2305-2312.

12. Dixon, Sidney C.; Miserentino, Robert; and Hudson, M. Latrelle: Theoretical and Experimental Vibration and Buckling Results for Blunt Truncated Conical Shells With Ring-Supported Edges. NASA TN D-7003, 1970.

13. Voss, H. M.: The Effect of an External Supersonic Flow on the Vibration Characteristics of Thin Cylindrical Shells. J. Aerosp. Sci., vol. 28, no. 12, Dec. 1961, pp. 945-956, 961.

14. Olson, Mervyn D.; and Fung, Y. C.: Comparing Theory and Experiment for the Supersonic Flutter of Circular Cylindrical Shells. AIAA J., vol. 5, no. 10, Oct. 1967, pp. 1849-1856.

15. Cohen, Gerald A.; Foster, Richard M.; and Dowty, James R.: Synthesis of Optimum Structural Designs for Conical and Tension Shell Mars Entry Capsules. NASA CR 1365, 1969.

16. Dugundji, John: Theoretical Considerations of Panel Flutter at High Supersonic Mach Numbers. AIAA J., vol. 4, no. 7, July 1966, pp. 1257-1266.

17. Ames Research Staff: Equations, Tables, and Charts for Compressible Flow. NACA REP. 1135, 1953. (Supersedes NACA TN 1428.)

18. Miserentino, Robert; and Dixon, Sidney C.: Vibration and Flutter Tests of a Pressurized Thin-Walled Truncated Conical Shell. NASA TN D-6106, 1971.

19. Comm. on Metric Pract.: ASTM Metric Practice Guide. NBS Handbook 102, U.S. Dep. Com., Mar. 10, 1967.

TABLE I.- PROPERTIES OF TYPICAL AEROSHELLS

Property	Ring-stiffened shell		Sandwich shell	
	Ring			
	Forward	Aft	Forward	Aft
EA	12.79 MN (2.875×10^6 lbf)	44.4 MN (9.98×10^6 lbf)	30.6 MN (6.89×10^6 lbf)	43.4 MN (9.76×10^6 lbf)
EI_x	3.42 kN-m^2 (1.193×10^6 lbf-in^2)	302 kN-m^2 (1.051×10^8 lbf-in^2)	3.70 kN-m^2 (1.29×10^6 lbf-in^2)	370 kN-m^2 (1.29×10^8 lbf-in^2)
EI_y	1.16 kN-m^2 (0.405×10^6 lbf-in^2)	302 kN-m^2 (1.051×10^8 lbf-in^2)	24.3 kN-m^2 (8.48×10^6 lbf-in^2)	262 kN-m^2 (9.13×10^7 lbf-in^2)
EI_{xy}	1.74 kN-m^2 (0.606×10^6 lbf-in^2)	0	-1.66 kN-m^2 (-5.8×10^5 lbf-in^2)	-43.9 kN-m^2 (-1.53×10^7 lbf-in^2)
GJ	78.3 N-m^2 (2.73×10^4 lbf-in^2)	228 kN-m^2 (7.96×10^7 lbf-in^2)	19.9 N-m^2 (6.95×10^3 lbf-in^2)	187 kN-m^2 (6.5×10^7 lbf-in^2)
z_o	-0.3239 cm (-0.1275 in.)	-11.7 cm (-4.61 in.)	-1.08 cm (-0.427 in.)	-9.75 cm (-3.48 in.)
Mass	3 kg (7 lbm)	39 kg (85 lbm)	7 kg (16 lbm)	42 kg (92 lbm)
	Shell			
α	60^o		60^o	
R_1	86.9 cm (34.2 in.)		86.9 cm (34.2 in.)	
R_2	290 cm (114 in.)		290 cm (114 in.)	
h_w	0.107 cm (0.042 in.)			
h_c			2.41 cm (0.947 in.)	
h_f			0.041 cm (0.016 in.)	
E	64.5 GN/m^2 (9.35×10^6 lbf/in^2) (includes rings)		64.5 GN/m^2 (9.35×10^6 lbf/in^2)	
μ	0.32		0.32	
γ	5.20 kg/m^2 (0.0074 lbm/in^2)		4.25 kg/m^2 (0.006 lbm/in^2)	
	Interior ring			
E	64.5 GN/m^2 (9.35×10^6 lbf/in^2)			
I_x	1.011 cm^4 (0.0243 in^4)			
I_y	0.153 cm^4 (0.00367 in^4)			
J	0.0011 cm^4 (0.000027 in^4)			
A	3.33 cm^2 (0.08 in^2)			
z_c	0.8362 cm (0.3292 in.)			
z_s	1.062 cm (0.4183 in.)			
d	6.15 cm (2.42 in.)			

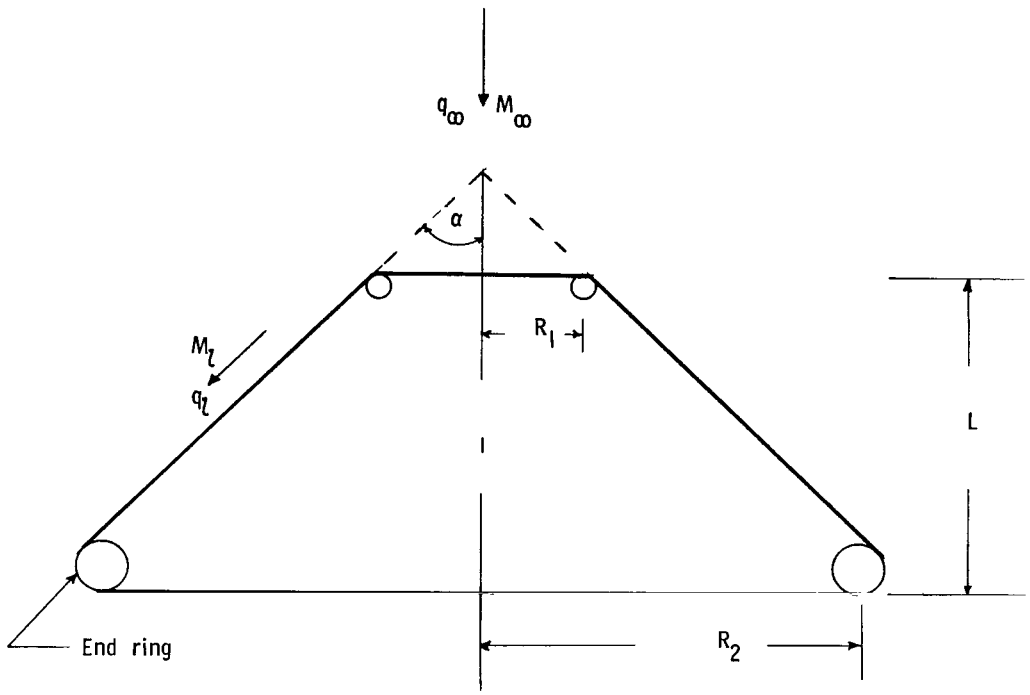

Figure 1.- Shell geometry.

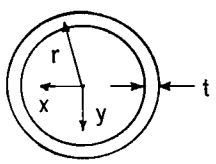

$$I_x = I_y = \pi r^3 t$$

$$I_{xy} = 0$$

$$J = 2I_x$$

$$A = 2\pi rt$$

$$r_1/r_2 = t_1/t_2 = R_1/R_2$$

$$t_2/h = 1$$

$$(z_0/r)_1 = (z_0/r)_2 = -1$$

Figure 2.- Pertinent dimensions and properties of end rings.

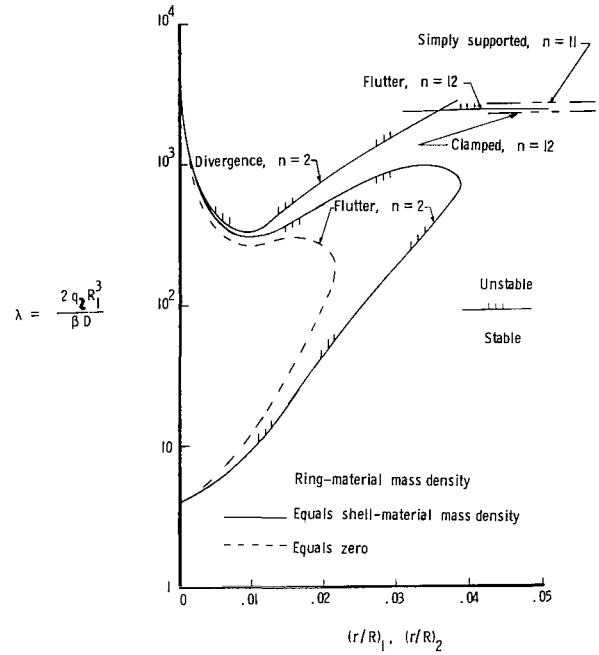

Figure 3.- Flutter characteristics of truncated conical shell with ring-supported edges. $L/R_1 = 2$; $R_1/h_w = 200$; $\alpha = 30^o$; $g_a = C_p = 0$.

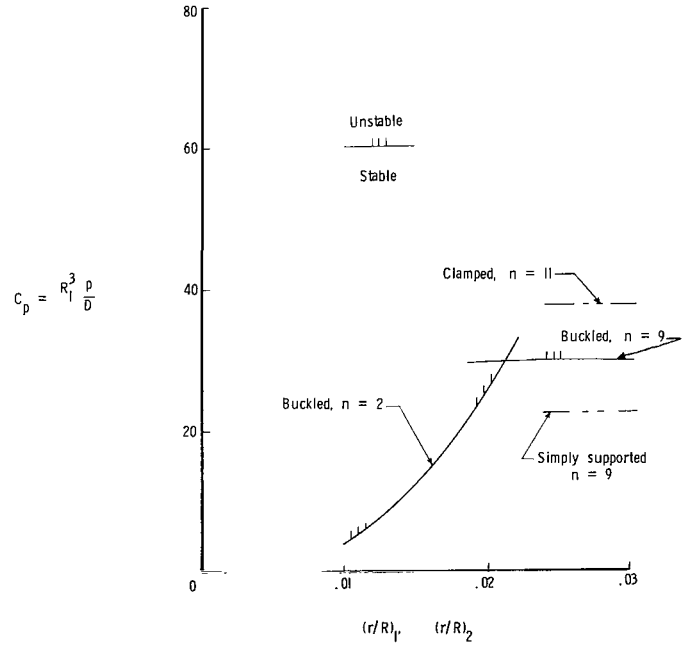

Figure 4.- Variation of buckling characteristics with ring size for truncated conical shell with ring-supported edges subjected to hydrostatic pressure. $L/R_1 = 2$; $R_1/h_w = 200$; $\alpha = 30^o$.

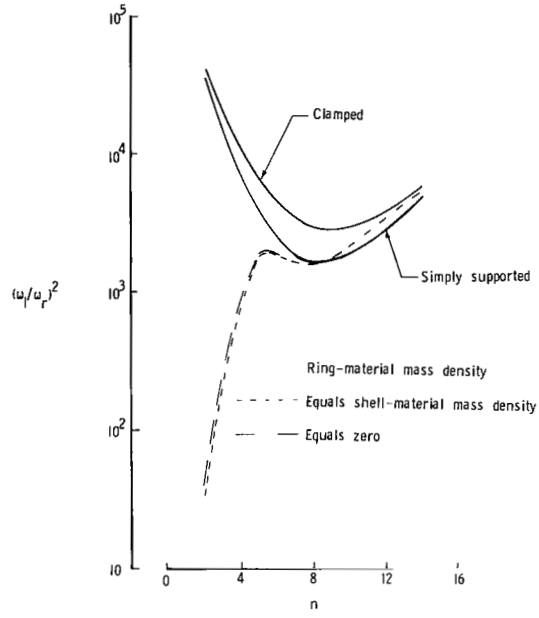

Figure 5.- Variation of natural frequencies with circumferential wave number for truncated conical shell with end rings sized from buckling considerations to provide edge restraint between restraint provided by simple and clamped support. $(r/R)_1 = (r/R)_2 = 0.021$; $L/R_1 = 2$; $R_1/h_w = 200$; $\alpha = 30^o$; $C_p = 0$.

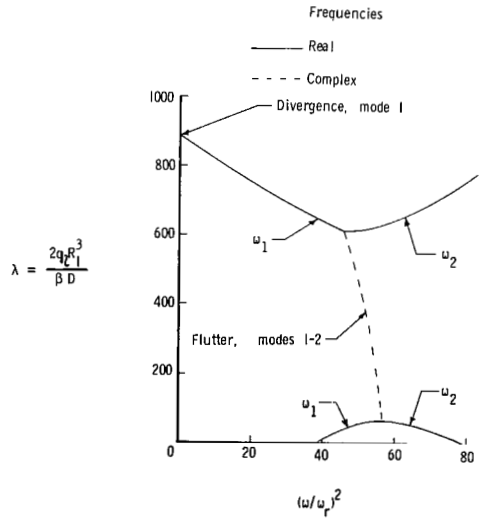

Figure 6.- Variation of natural frequencies with airflow where instability changes from a mode 1-2 flutter to a mode 1 divergence. Ring-material mass density equals shell-material mass density; $L/R_1 = 2$; $R_1/h_w = 200$; $(r/R)_1 = (r/R)_2 = 0.021$; $n = 2$; $\alpha = 30^o$; $g_a = C_p = 0$.

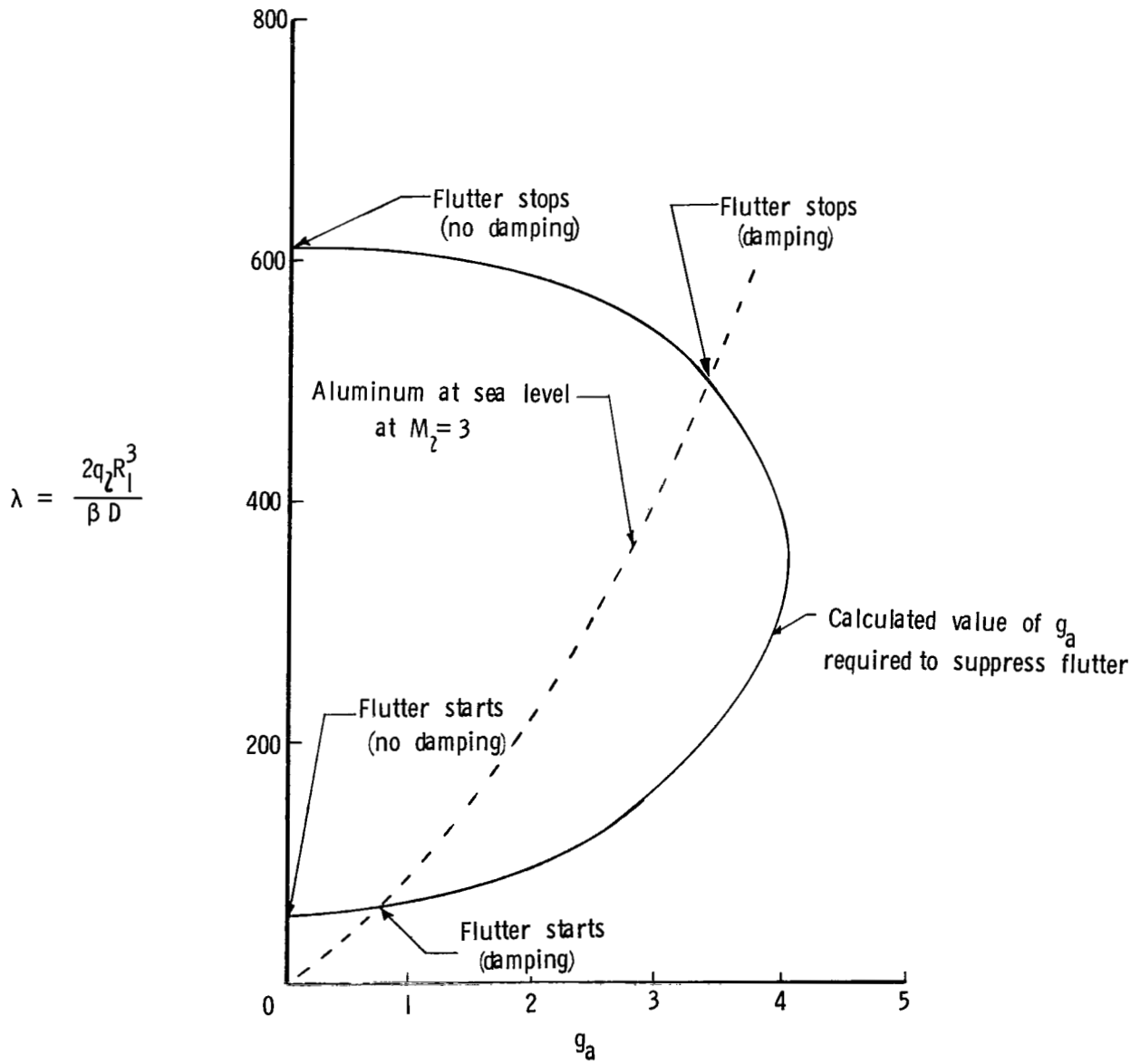

Figure 7.- Effect of aerodynamic damping where instability changes from a mode 1-2 flutter to a mode 1 divergence. Ring-material mass density equals shell-material mass density; $L/R_1 = 2$; $R_1/h_w = 200$; $(r/R)_1 = (r/R)_2 = 0.021$; $n = 2$; $\alpha = 30^o$; $C_p = 0$.

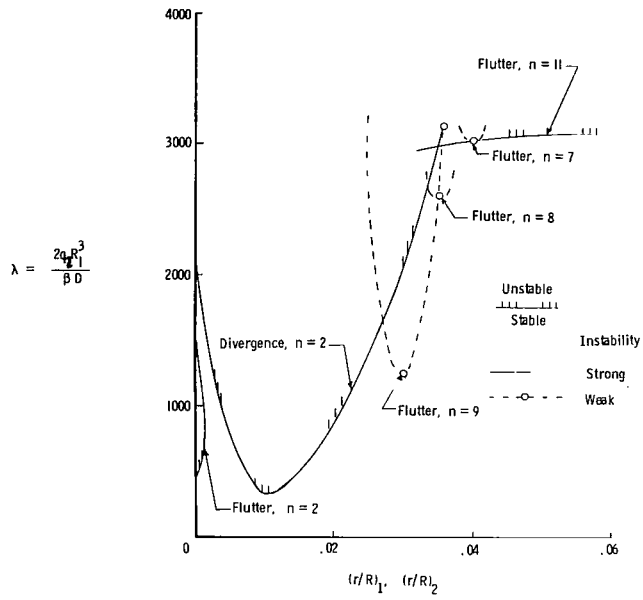

(a) $\alpha = 10^{\circ}$.

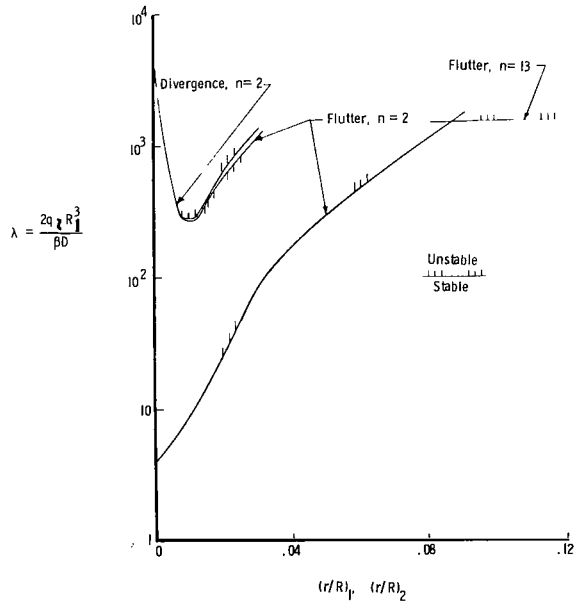

(b) $\alpha = 45^{\circ}$.

Figure 8.- Effects of cone angle on flutter characteristics of truncated conical shell with ring-supported edges. Ring-material mass density equals shell-material mass density; $L/R_1 = 2$; $R_1/h_w = 200$; $g_a = C_p = 0$.

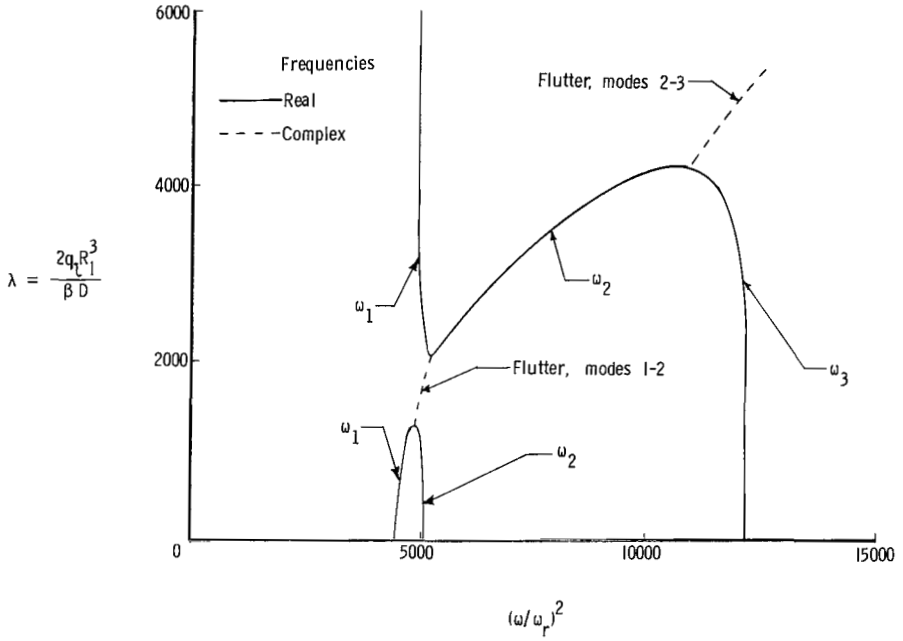

Figure 9.- Variation of natural frequencies with airflow where flutter changes from a mode 1-2 instability to a mode 2-3 instability. Ring-material mass density equals shell-material mass density; $L/R_1 = 2$; $R_1/h_w = 200$; $(r/R)_1 = (r/R)_2 = 0.03$; $n = 9$; $\alpha = 10^o$; $g_a = C_p = 0$.

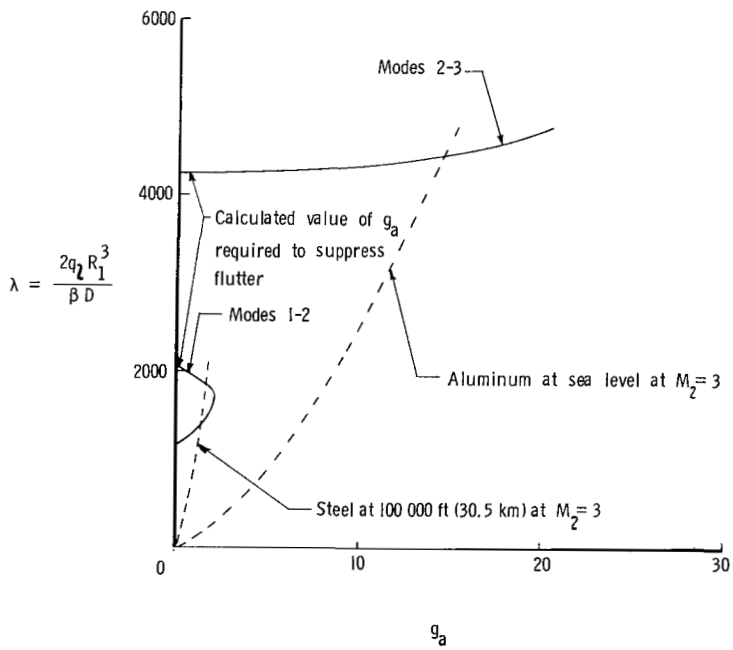

Figure 10.- Effect of aerodynamic damping where flutter changes from a mode 1-2 instability to a mode 2-3 instability. Ring-material mass density equals shell-material mass density; $L/R_1 = 2$; $R_1/h_w = 200$; $(r/R)_1 = (r/R)_2 = 0.03$; $n = 9$; $\alpha = 10^o$; $C_p = 0$.

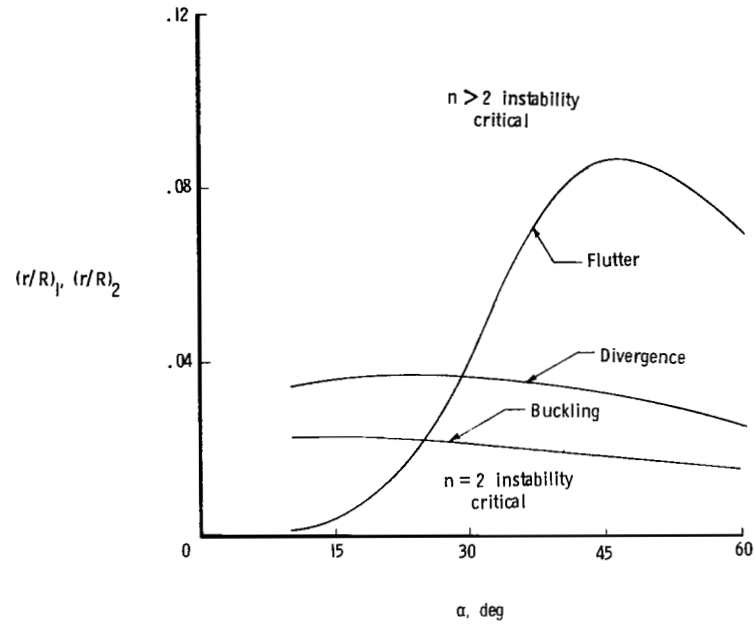

Figure 11.- Variation of minimum ring-shell-radius ratio required to prevent the $n = 2$ mode as the governing instability with cone angle α. $L/R_1 = 2$; $R_1/h_w = 200$.

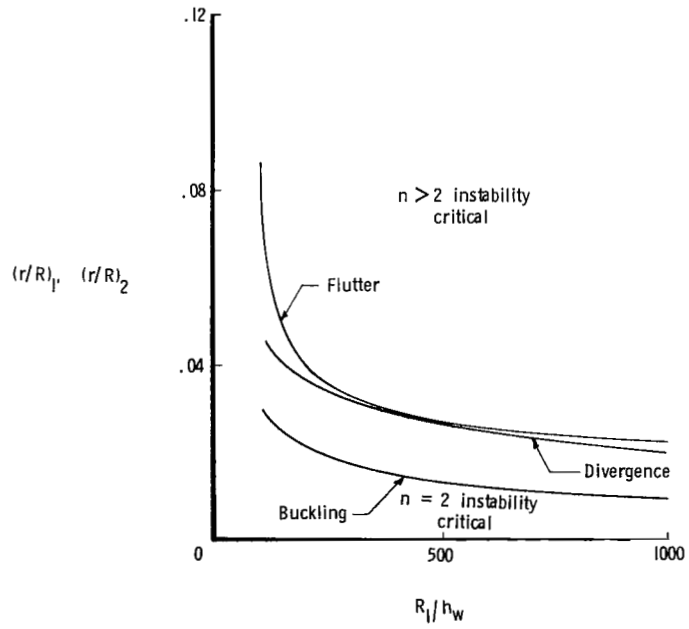

Figure 12.- Variation of minimum ring-shell-radius ratio required to prevent the $n = 2$ mode as the governing instability with shell radius-thickness ratio R_1/h_w. $L/R_1 = 2$; $\alpha = 30^o$.

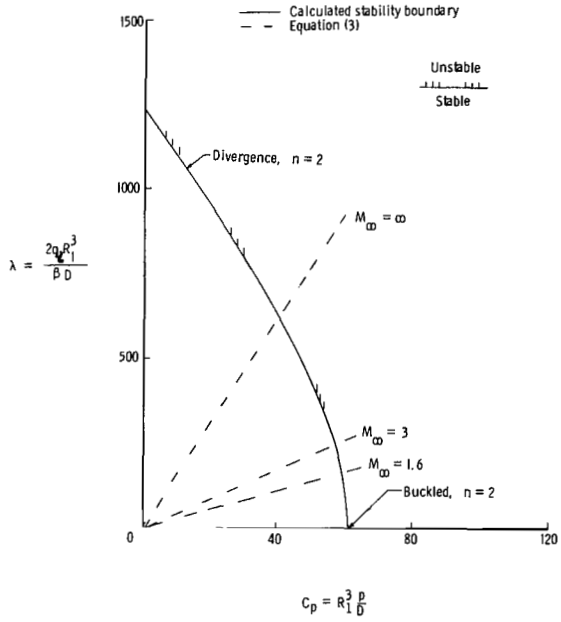

(a) $\alpha = 10^o$; $(r/R)_1 = (r/R)_2 = 0.0264$.

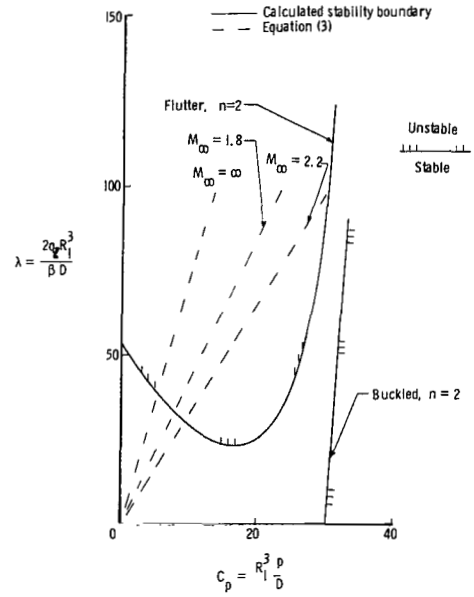

(b) $\alpha = 30^o$; $(r/R)_1 = (r/R)_2 = 0.021$.

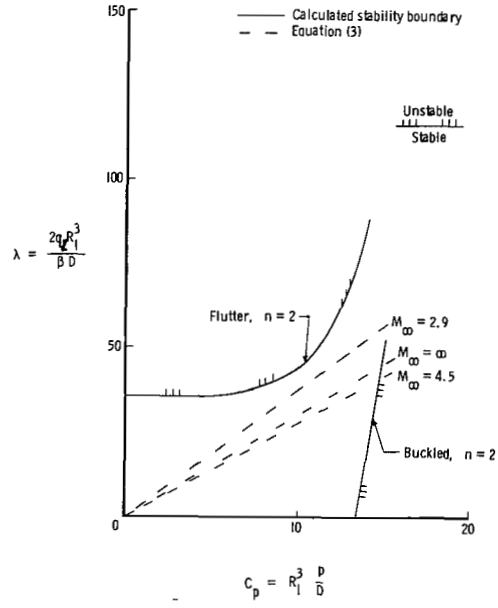

(c) $\alpha = 45^o$; $(r/R)_1 = (r/R)_2 = 0.0172$.

Figure 13.- Stability characteristics of ring-supported conical shells subjected to external airflow and external pressure loading. Ring-material mass density equals shell-material mass density. $L/R_1 = 2$; $R_1/h_w = 200$; $g_a = 0$.

NASA-Langley, 1971 —— 32 L-7527

"The aeronautical and space activities of the United States shall be conducted so as to contribute . . . to the expansion of human knowledge of phenomena in the atmosphere and space. The Administration shall provide for the widest practicable and appropriate dissemination of information concerning its activities and the results thereof."

— NATIONAL AERONAUTICS AND SPACE ACT OF 1958

NASA SCIENTIFIC AND TECHNICAL PUBLICATIONS

TECHNICAL REPORTS: Scientific and technical information considered important, complete, and a lasting contribution to existing knowledge.

TECHNICAL NOTES: Information less broad in scope but nevertheless of importance as a contribution to existing knowledge.

TECHNICAL MEMORANDUMS: Information receiving limited distribution because of preliminary data, security classification, or other reasons.

CONTRACTOR REPORTS: Scientific and technical information generated under a NASA contract or grant and considered an important contribution to existing knowledge.

TECHNICAL TRANSLATIONS: Information published in a foreign language considered to merit NASA distribution in English.

SPECIAL PUBLICATIONS: Information derived from or of value to NASA activities. Publications include conference proceedings, monographs, data compilations, handbooks, sourcebooks, and special bibliographies.

TECHNOLOGY UTILIZATION PUBLICATIONS: Information on technology used by NASA that may be of particular interest in commercial and other non-aerospace applications. Publications include Tech Briefs, Technology Utilization Reports and Technology Surveys.

Details on the availability of these publications may be obtained from:

SCIENTIFIC AND TECHNICAL INFORMATION OFFICE

NATIONAL AERONAUTICS AND SPACE ADMINISTRATION

Washington, D.C. 20546